# Simplified Stability Analysis Method for Multiple Servo Drive Systems Connected to Common DC Bus Line


Katsuki Miura
Dept. of Electrical, Electronics, and Information Engineering
Nagaoka University of Technology
Nagaoka, Japan
k_miura@stn.nagaokaut.ac.jp

Hiroki Watanabe
Dept. of Electrical, Electronics, and Information Engineering
Nagaoka University of Technology
Nagaoka, Japan
hwatanabe@vos.nagaokaut.ac.jp

Keisuke Kusaka
Dept. of Electrical, Electronics, and Information Engineering
Nagaoka University of Technology
Nagaoka, Japan
kusaka@vos.nagaokaut.ac.jp

Jun-ichi Itoh
Dept. of Electrical, Electronics, and Information Engineering
Nagaoka University of Technology
Nagaoka, Japan
itoh@vos.nagaokaut.ac.jp

Takeshi Kiribuchi
OMRON Corporation
Kyoto, Japan
takeshi.kiribuchi@omron.com

Hiroyuki Tokusaki
OMRON Corporation
Kyoto, Japan
hiroyuki.tokusaki@omron.com



***Abstract*— This paper proposes a simplified stability analysis method based on Middlebrook's method for multiple servo drive systems connected to the DC-bus line with the line inductance and resistance. The impedance of the DC-bus line causes interference among each current-control bandwidth for the motor. This paper reveals the relationship between the multiple servo drive systems stability limit and the DC-bus impedance with the simplified stability analysis method. The validity of the proposed method is demonstrated by comparison with the mathematical analysis and experiment results. As a result, the stability limit calculated by the proposed method is matched within an error of 2%. This paper also clarifies the cause of the errors between the mathematical analysis results and the experimental results in terms of regarding system loss.**



***Keywords— DC-Bus System, Servo Drive, Impedance-based Stability Analysis***


## I. INTRODUCTION

In recent years, servo-drive systems have been used widely in industrial applications. It is generally required to achieve high control performance, low noise, and high power density[1-5]. In the conventional configuration of the servo drive systems, the control panel, including servo drivers and servo motors, are connected by AC lines. However, the conventional configuration has a problem which is a radiated switching noise from AC lines. Thus, countermeasures are needed to prevent interference from other pieces of equipment such as shielding lines and the layout of power and signal lines. However, the costs are increased due to the countermeasure for the noises.

In order to solve this problem, the DC-bus servo drive system, which connects the servo driver to the DC-bus line, has been attracted [6]. This configuration reduces the radiation noise due to the shorter length of the three-phase power line cables and the loss due to no rectifier stage. Moreover, the DC-bus servo drive systems prevent the complicated wiring and reduce the cost of the noise suppression since the number of long power lines.

However, the DC-bus servo drive systems have the problem of system instability due to the interference between the line impedance of the DC-bus and the current control band for the motor [7-13]. The over-voltage protection will trip the system due to oscillation in the bus current and DC-link capacitors voltage when the DC-bus servo drive system is unstable. This interference occurs due to the negative resistance characteristics of the servo driver, which is a constant power load. Also, the system stability is wrong when the servo driver's small DC-link capacitance is used to achieve high power density [14-16]. Therefore, the stability analysis and damping control method for the DC-bus servo drive systems are required. The stability analysis method for the DC-bus system is proposed by Middlebrook [17]. In Middlebrook's analysis method, the system is divided into source and load sides. The system stability is analyzed by the Nyquist plot of the product of the output impedance of the source side and the input admittance on the load side. Ref. [6] has derived the input admittance of the servo driver by the extra element theorem and proposed the stability analysis method for the DC-bus servo drive system based on Middlebrook's method. However, the stability of the multiple DC-bus servo drive system is not discussed in Ref. [6], although there are many situations to use many servo drivers in a DC-bus line. In particular, the relationship between DC line impedances and stability limit is unclear.

This paper proposes a simple stability analysis method for multiple DC-bus servo drive systems. The new contribution of this paper is that the relationship between the system stability and the line impedance of the DC-bus is clarified by a simple equation based on Middlebrook's method. The validity of the proposed analysis method is evaluated by the analysis results using a full-order state equation and experimental results. The stability limit calculated by the proposed analysis agrees with that of the state equation analysis within 2%. Furthermore, this paper discusses the influence of not only the DC-bus line but also the line between the DC-bus and each servo driver because the proposed analysis method is based on the condition that the DC-bus line is longer than the line between the DC-bus and each servo driver. In addition, the stability limit calculated by the

proposed analysis method is evaluated by the operating condition of the servo motors in the experiment. As a result, the stability limit in the proposed analysis agrees with that in the experiment within 11% of the rated power. Moreover, the cause of the error is also discussed with the system losses of the experimental setup.

## II. System Configuration of DC-Bus Servo Drive System

### A. Circuit configuration

Fig. 1 shows the system configuration of the DC-bus servo drive system analyzed in this paper. Table 1 shows the circuit parameters of the analyzed system. Fig. 1 shows that two servo drivers are connected to a common DC bus with long lines. Note that this model consists of two servo drivers for simplification of the following analysis. In Fig. 1, $L_{bus}$ is the line impedance of the DC-bus, $R_{bus}$ is the line resistance of the DC-bus, $L_{b1}$ and $L_{b2}$ are the line impedances between the DC-bus and each servo driver, $R_{b1}$ and $R_{b2}$ are the line resistances between the DC-bus and each driver, $C_{b1}$ and $C_{b2}$ are the DC-link capacitors of the servo driver. The value of the input capacitance of the servo driver is small in order to achieve high power density. Note that line impedance is included in the DC-bus line and the line between the DC-bus and each unit.

### B. Controller configuration

Fig. 2 shows the control block diagram of each servo driver with Field-Oriented Control (FOC). The PI controller is used for the current control of the d-axis and q-axis. In addition, the zero d-axis current control and the feed-forward compensation for canceling the interference of the permanent magnetic(PM) motor are applied.

The transfer function of the PI controller $PI(s)$ is expressed as

$$PI(s) = K_p\left(1+\frac{1}{sT_i}\right) \quad (1),$$

where $K_p$ is the proportional gain, and $T_i$ is the integration time. $K_p$ and $T_i$ are designed to cancel the zero point in the closed transfer function of the current control. The proportional gain $K_p$ and the integration time $T_i$ are expressed as

$$\begin{cases} K_p = \omega_c L_m \\ T_i = L_m / R_a \end{cases} \quad (2),$$

where $\omega_c$ is the cutoff angular frequency of the current controller.

### C. State equation of the DC-bus servo drive system with long lines

The equivalent small-signal model of this system approximated near the operating point is expressed as an eighth-order state equation. The state equation of the analyzed system is expressed as

$$\frac{d}{dt}\begin{bmatrix} \Delta i_{b1} \\ \Delta v_{b1} \\ \Delta i_{in1} \\ \Delta v_{\mathrm{int}1} \\ \Delta i_{b2} \\ \Delta v_{b2} \\ \Delta i_{in2} \\ \Delta v_{\mathrm{int}2} \end{bmatrix} = \begin{bmatrix} A_{11} & A_{12} & 0 & 0 & A_{15} & A_{16} & 0 & 0 \\ A_{21} & 0 & A_{23} & 0 & 0 & 0 & 0 & 0 \\ 0 & A_{32} & A_{33} & A_{34} & 0 & 0 & 0 & 0 \\ 0 & A_{42} & A_{43} & 0 & 0 & 0 & 0 & 0 \\ A_{51} & A_{52} & 0 & 0 & A_{55} & A_{56} & 0 & 0 \\ 0 & 0 & 0 & 0 & A_{65} & 0 & A_{67} & 0 \\ 0 & 0 & 0 & 0 & 0 & A_{76} & A_{77} & A_{78} \\ 0 & 0 & 0 & 0 & 0 & A_{86} & A_{87} & 0 \end{bmatrix} \begin{bmatrix} \Delta i_{b1} \\ \Delta v_{b1} \\ \Delta i_{in1} \\ \Delta v_{\mathrm{int}1} \\ \Delta i_{b2} \\ \Delta v_{b2} \\ \Delta i_{in2} \\ \Delta v_{\mathrm{int}2} \end{bmatrix} + \begin{bmatrix} B_1 \\ 0 \\ 0 \\ 0 \\ B_5 \\ 0 \\ 0 \\ 0 \end{bmatrix} \Delta v_{dc} \quad (3),$$

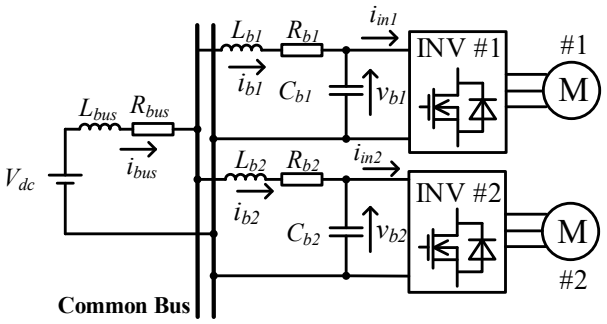


Fig .1 Analyzed system configuration of DC-bus servo drive system with two servo drivers connected to the DC-bus.

TABLE 1 Analyzed circuit parameters.

| | | |
|---|---|---|
| | Circuit | |
| $L_{bus}$ | Wiring indutance of DC Bus | 1 mH |
| $R_{bus}$ | Wiring resistance of DC Bus | 0.02 Ω |
| $C_{b1}$, $C_{b2}$ | Inverter input capasitance | 13 μF |
| $V_{dc}$ | DC bus voltage | 280 V |
| | Motor (#1, #2) | |
| $R_a$ | Wiring resistance | 1.4 Ω |
| $L_a$ | Wiring inductance | 3.41 mH |
| $K_e$ | Back-EMF constant | 0.051 V/(rad･s) |
| $P_f$ | Pole pairs | 5 |

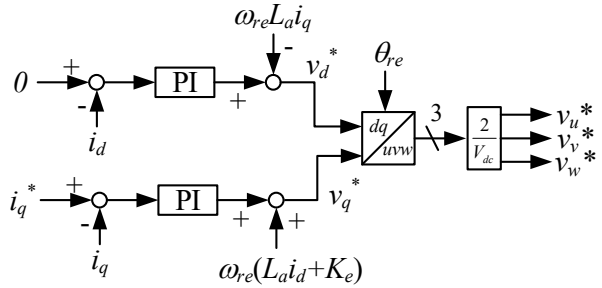


Fig. 2 Control block diagram with the Field Oriented Control (FOC) in each controller. Zero d-axis current control and feed-forward compensation for canceling the interference of the PM motor are applied.

where each element of the state equation are in the appendix. There are four state variables per unit. The state variables are as follows;

$\Delta i_{b1}$, $\Delta i_{b2}$: Current flowing through the wiring inductance between the DC bus and the inverter.

$\Delta v_{b1}$, $\Delta v_{b2}$: Inverter input capacitor voltage.

$\Delta i_{in1}$, $\Delta i_{in2}$: Motor q-axis current converted to DC side of the inverter.

$\Delta v_{int1}$, $\Delta v_{int2}$: Integral value of the PI controller.

The state equation of the current flowing into unit #1 ($\Delta i_{b1}$) includes another unit state variable ($\Delta i_{b2}$, $\Delta v_{b2}$). In addition, each element, such as $A_{11}$, $A_{12}$, $A_{15}$, $A_{16}$, and $B_1$, includes the bus impedance ($L_{bus}$, $R_{bus}$) and the line impedance of other

units ($L_{b2}$, $R_{b2}$). Therefore, interference among each unit connected to the DC-bus occurs in this system.

The analysis method by the state equation of the whole system is difficult when many units are connected to the DC-bus line due to the complexity of deriving the state equation.

In this paper, the interference among each unit is analyzed by assuming that the line from DC-bus to the servo driver is sufficiently longer than the DC-bus line. The state equation of the current flowing into unit #1 from the DC-bus when $L_{bus} << L_{b1}$, $L_{b2}$, and $R_{bus} << R_{b1}$, $R_{b2}$ is approximated as

$$\frac{\Delta i_{b1}}{dt} \cong -\frac{R_{b1}}{L_{b1}}\Delta i_{b1} - \frac{1}{L_{b1}}\Delta v_{b1} + \frac{1}{L_{b1}}\Delta v_{dc} \quad (4).$$

Equation (4) does not include other unit state variables and parameters. Therefore, the interference among each unit connected to DC-bus does not occur under the condition that the line between the DC-bus and the servo driver is sufficiently longer than the DC-bus line. In this case, it is possible to analyze the stability of the whole system by the Middlebrook method for each unit.

## III. Proposed Stability Analysis Method

In this section, the stability analysis method with the case that the impedance of the DC-bus is larger than the line impedance between the DC-bus and the unit is proposed. This proposed analysis method is based on the impedance method proposed by Middlebrook [17].

### A. The impedance model

Fig. 3 shows the equivalent impedance model when the line impedance of the DC-bus is larger than the line impedance between the DC-bus and each unit. In this model, the servo driver is expressed as the input admittance $Y_{in1}(s)$, $Y_{in2}(s)$. The equivalent impedance model is expressed as a model in that the LC filter and the input admittance of the servo driver are cascaded.

The output impedance of the LC filter $Z_o(s)$ is expressed as

$$Z_o(s) = \frac{sL_{bus} + R_{bus}}{s^2 L_{bus} C_{bus} + sC_{bus} R_{bus} + 1} \quad (5),$$

where $C_{bus}$ is the sum of the input capacitance of the servo drivers.

The input admittance of each servo driver $Y_{in}(s)$ is derived by the extra element theorem [6]. The input admittance of a constant power load is expressed as

$$Y_{in}(s) = \frac{1}{Z_N(s)}\frac{T(s)}{1+T(s)} + \frac{1}{Z_D(s)}\frac{1}{1+T(s)} \quad (6),$$

where $Z_N(s)$ is the input impedance with ideal feedback, $Z_d(s)$ is the input impedance without feedback, and $T(s)$ is the open-loop transfer function of the current control loop. The input impedance without feedback $Z_D(s)$ is expressed as

$$Z_D(s) = \frac{1}{\alpha^2}\left(R_a + sL_m\right) = \left(\frac{V_{b,0}}{R_a I_{q,0} + \omega_{re} K_e}\right)^2 \left(R_a + sL_m\right) \quad (7),$$

where $\alpha$ is the conversion ratio, $I_{q,0}$ is the steady-state value of q-axis current, $\omega_{re}$ is the motor angular velocity, and $V_{b,0}$ is the steady-state value of the servo driver input voltage. The load impedance of the motor is converted to the input impedance by the conversion ratio.

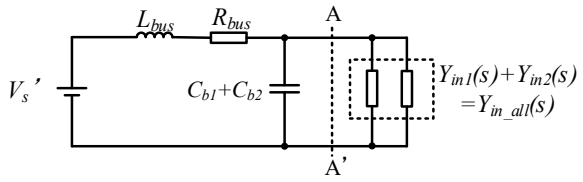


Fig. 3 The equivalent impedance model when the line impedance of the DC-bus is larger than the line impedance between the DC-bus and each unit.

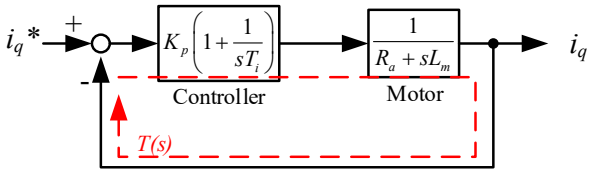


Fig. 4 The simplified system block diagram. This model ignores the interference term and d-axis current control loop due to feed-forward compensation and zero d-axis current control.

The input impedance with ideal feedback $Z_N(s)$ is expressed as

$$Z_N(s) = -\frac{V_{b,0}}{I_{b,0}} = -\frac{V_{b,0}^2}{P_{out}} = -\frac{V_{b,0}^2}{\left(I_{q,0}R_a + \omega_{re}K_e\right)I_{q,0}} \quad (8),$$

where $I_{b,0}$ is the steady-state value of the DC-link current, and $P_{out}$ is the motor output. Note that $Z_N(s)$ is a negative impedance depending on the motor output power.

Fig. 4 shows the simplified system block diagram. The system block diagram in fig. 4 ignores the d-axis current control loop and the interference term of the PM motor due to the feed-forward compensation and the zero d-axis current control. The open-loop transfer function of the current control loop $T(s)$ is expressed as

$$T(s) = PI(s)G(s) = K_p\left(1+\frac{1}{sT_i}\right)\frac{1}{R_a + sL_m} \quad (9),$$

where $G(s)$ is the transfer function of the motor.

The input admittance of the servo driver is expressed by substituting (7)-(9) for (6) as (10).

$$Y_{in}(s) = -\frac{I_{q,0}\left(R_a I_{q,0} + \omega_{re}K_e\right)}{V_{bus,0}^2}\frac{T(s)}{1+T(s)} + \frac{\left(R_a I_{q,0} + \omega_{re}K_e\right)^2}{V_{b,0}^2\left(R_a + sL_m\right)}\frac{1}{1+T(s)} \quad (10)$$

The servo driver input admittance consists of the negative term depending on the motor output and the positive term depending on the square of the output voltage. Thus, the input admittance of the servo motor changes with the operation points, such as torque (q-axis current) and motor speed.

### B. The proposed stability analysis method

The stability of the model shown in Fig. 3 is analyzed with the Nyquist plot of $T_{MLG}(\omega)$, which is the product of the output impedance of the LC filter $Z_o(s)$ and the combined input admittance of the servo driver $Y_{in\_all}(s)$. $T_{MLG}(\omega)$ is expressed as

$$T_{MLG}(\omega) = Z_o(\omega) \times Y_{in\_all}(\omega)$$
$$= \left[ \mathrm{Re}\{Z_o(\omega)\}\mathrm{Re}\{Y_{in\_all}(\omega)\} - \mathrm{Im}\{Z_o(\omega)\}\mathrm{Im}\{Y_{in\_all}(\omega)\} \right]$$
$$+ j\left[ \mathrm{Re}\{Z_o(\omega)\}\mathrm{Im}\{Y_{in\_all}(\omega)\} + \mathrm{Im}\{Z_o(\omega)\}\mathrm{Re}\{Y_{in\_all}(\omega)\} \right] \quad (11).$$

Figure 5 shows the Nyquist plots. The Nyquist stability criterion determines the system stability from the value of the real part of $T_{MLG}(\omega)$ at the angular frequency $\omega_o$ which the imaginary part is zero. The stability condition is expressed as

$$\left[ \mathrm{Re}\{Z_o(\omega_o)\}\mathrm{Re}\{Y_{in\_all}(\omega_o)\} - \mathrm{Im}\{Z_o(\omega_o)\}\mathrm{Im}\{Y_{in\_all}(\omega_o)\} \right] > -1 \quad (12).$$

However, it is difficult to solve the complicated equation of the imaginary part in $T_{MLG}(\omega)$ for $\omega_o$. Therefore, this paper proposes the simple stability analysis method using the resonant angular frequency of the LC filter $\omega_{res}$ instead of $\omega_o$. The resonant angular frequency of the LC filter $\omega_{res}$ is expressed as

$$\omega_{res} = \frac{1}{\sqrt{L_{bus}(C_{b1} + C_{b2})}} \quad (13).$$

Fig. 6 shows the relationship between $\omega_o$ and $\omega_{res}$ on the bode diagram and the Nyquist plot of $T_{MLG}(\omega)$. In Fig. 6 (a), $\omega_{res}$ and $\omega_o$ are close on the bode diagram because the phase of $T_{MLG}(s)$ is changed sharply near the resonant angular frequency of the LC filter. Fig. 6 (b) shows that $\mathrm{Re}\{T_{MLG}(\omega_o)\}$ is almost agreed with $\mathrm{Re}\{T_{MLG}(\omega_{res})\}$. Thus, the system stability is determined by the real part value of $T_{MLG}(\omega_{res})$. Note that the error between $\mathrm{Re}\{T_{MLG}(\omega_{res})\}$ and $\mathrm{Re}\{T_{MLG}(\omega_o)\}$ is dependent on the square of the ratio $R_{bus}$ to $L_{bus}$.

The stability condition equation is expressed by substituting the resonance angular frequency of LC filter $\omega_{res}$ for $\mathrm{Re}\{T_{MLG}(\omega_{res})\}$ as

$$\mathrm{Re}\{Y_{in\_all}(\omega_{res})\} > -\frac{R_{bus}(C_{b1} + C_{b2})}{L_{bus}} \quad (14).$$

The proposed analysis method expresses the stable condition by the equation, which consists of the real part of the combined input admittance of the servo drivers, the line inductance, the resistance of the DC-bus, and the input capacitor of the servo driver.

Fig. 7 shows the relationship between the output power of the servo motor and the real part of the input admittance of the servo driver. The stable condition by (14) is also shown in Fig. 7. The stability limit is expressed clearly by (14). The real part of $T_{MLG}(\omega_{res})$ is decreased linearly with increasing the motor output power. Besides, the stable output range when the motor rotates is expanded because the real part of $T_{MLG}(\omega_{res})$ is increased.

## IV. Analysis Results

In this section, the validity of the proposed analysis method is evaluated by comparison with the stable limit output calculated by the polar arrangement of (3). The analysis parameters are based on Table 1.

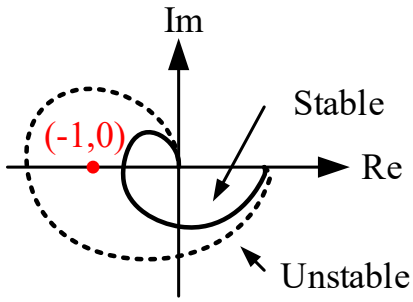


Fig. 5 The Nyquist plot. The system stability is determined by the real part value when the imaginary part is zero.

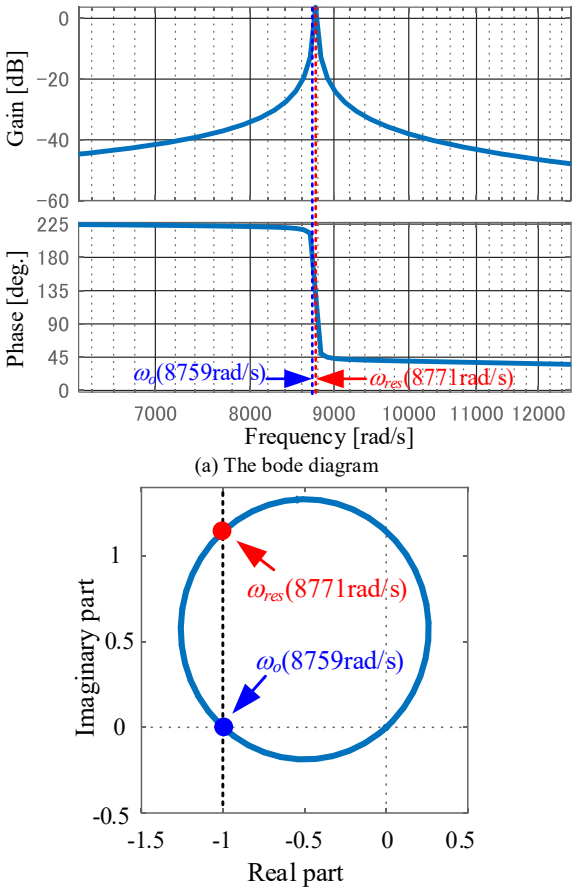


(a) The bode diagram

(b) The Nyquist plot.

Fig. 6 The relationship between $\omega_o$ and $\omega_{res}$. The real part value of $T_{MLG}(\omega_o)$ and $T_{MLG}(\omega_{res})$ are almost agreed.

### A. *Stability analysis when two motors are driven.*

Fig. 8 shows the pole map of the state equation in the DC-bus servo drive system by (3) when unit #1 is driven at 200 W, 3000 r/min, and unit #2 is driven at 1500 r/min. The poles of the system move to the right half-plane (RHP) by increasing the q-axis current of unit #2. When the q-axis current of unit #2 is larger than 1.92 A, the poles are located in the RHP. It means the system is unstable.

Fig. 9 shows the stability limit calculated by the proposed and full-order state equation analysis methods when two servo drivers are connected to the DC-bus. Note that unit #1 is driven at 3000 r/min, and unit #2 side motor is driven at 1500 r/min. The stability limit of single-unit changes depending on

the output power of another unit. The stability limit calculated by the proposed analysis agrees with the state equation analysis within 2%. Therefore, the proposed simple analysis method determines the stability of the DC-bus servo drive system with high accuracy.

### *B. The influence of the line between the DC-bus and each unit*

The proposed analysis method is based on the condition that the DC-bus line is sufficiently longer than the line between the DC-bus and each unit. This section discusses the influence of the line impedance between the DC-bus and each unit on the accuracy of the proposed analysis method.

Fig. 10 shows the error ratio of the stable limit between the proposed analysis method and the full-order state equation when the ratio of the DC-bus line inductance to the line inductance between the DC-bus and each unit is changed. Also, the value of $R_{b1}$ is changed so that the ratio of $L_{b1}/R_{b1}$ is the same. In addition, the line impedance of unit #2 ($L_{b2}$, $R_{b2}$) are same as unit #1 as the line length between the DC-bus and each unit is equal. These conditions are that the stable limit output of unit #2 is compared when unit #1 output is 200 W. In Fig. 10, the error ratio of the calculated stable limit between the proposed analysis method and the full-order state equation is increased with an increased ratio $L_{b1}/L_{bus}$. When the ratio $L_{b1}/L_{bus}$ is 1/10, the proposed analysis method determines the system's stability within 1% compared to the state equation method.

## V. Experimental Results

Table 1 shows the experimental conditions. Note that the line resistance of the DC-bus $R_{bus}$ includes the DC and AC resistance at the resonant frequency of the LC filter. The inductance and AC resistance of the line inductor is measured with an LCR meter (HIOKI 3522-50). Also, DC resistance is measured by the voltage drop calculation method. The load-side motor controls each servo motor rotation speed. The stable limit is searched by changing the q-axis current command of the tested servo system.

Fig. 11 shows the bus current waveform and input capacitor voltage waveform of each unit when the q-axis current command value on unit #2 is increased. The oscillation occurs in the bus current and capacitor voltage when the system is unstable. Note that unit #1, which does not change the operating point, becomes unstable due to interference among each unit.

Fig. 12 shows the stability limit by the proposed analysis method and the experimental result with two units. The motor of unit #1 rotates 3000 r/min, and that of unit #2 rotates 1500 r/min. From Fig. 10, the result of the analysis and experimental shows that the stable limit of one unit is reduced by increasing the output of another unit. However, the stability limit of the experiment is increased by 42 W on average, 11% of the rated output power, compared with the stability limit by the proposed method.

Fig. 13 shows the simulation circuit model with the inverter loss. The simulation, including the inverter and motor losses, is performed in order to discuss the cause of the error between the experimental result and the analysis result. The inverter loss is simulated by inserting the variable resistor based on efficiency characteristics into the DC side of the

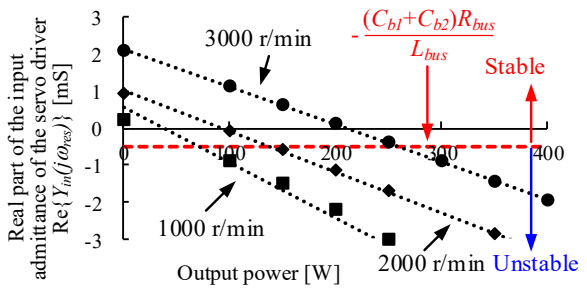


Fig. 7 The relationship between motor output and the real part of the servo input admittance. The stable condition is also shown. The real part value of $T_{MLG}(\omega)$ at the resonant angular frequency $\omega_{res}$ is decreased linearity with increasing output power.

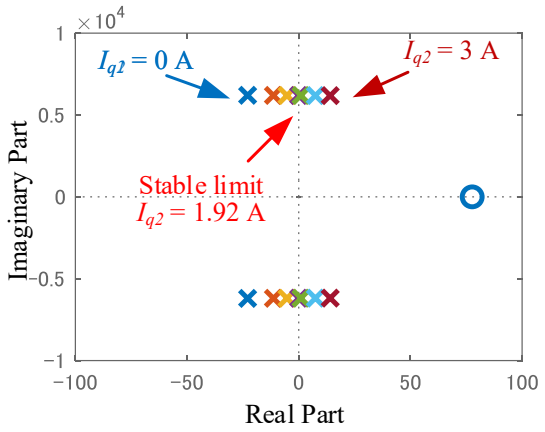


Fig. 8 The pole map of the DC-bus servo drive system when unit #1 is driven at 200 W, 3000 r/min, and #2 is driven at 1500 r/min.

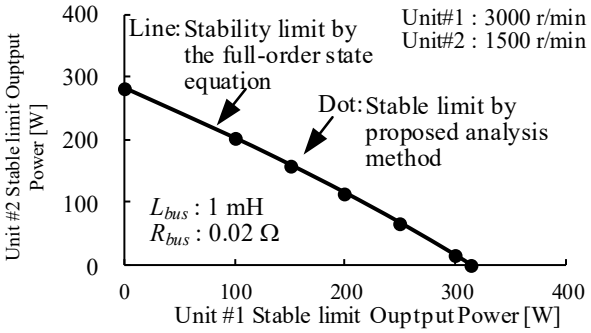


Fig. 9 The relationship of the stable limit power at two motors connected DC bus. The stable limit of single-unit changes depending on the output power of another unit.

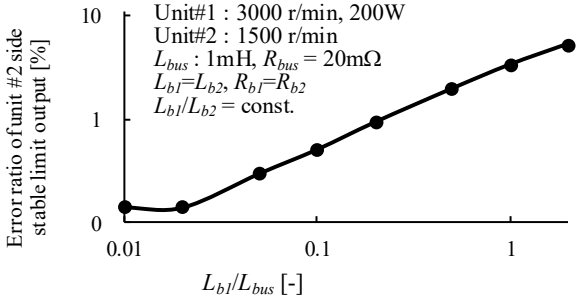


Fig. 10 The stable limit power error relationship between the proposed analysis method and analysis by state equation when the line inductance between the DC-bus and each unit is changed. The resistance value is also changed so that the ratio.

servo driver. The efficiency of the servo motor is measured by a power meter (HIOKI PW6001). The simulation model also includes deadtime and discretized control systems.

Fig. 14 shows the stability limit when a motor is driven as calculated by the proposed analysis method, the simulation result, and the experimental result. The error between the simulation result and the experimental result is reduced by approximately 50%. Therefore, the losses of the inverter and motor also influence the stability of the DC-bus servo drive system.

## VI. Conclusions

This paper proposed the simple stability analysis method of the DC-bus servo drive system. The proposed method clarified the influence of the line impedance of the DC-bus on the stability of the DC-bus servo drive system. The stability limit calculated by the proposed method agreed with the result of the full-order state equation analysis method to within 2%. The influence of the line impedance between the DC-bus and each unit for the accuracy of the proposed analysis method is also discussed. In addition, the stability limit by the proposed method agreed with 11% of the rated power by experimental result. The cause of error between the analysis result and the experimental result is discussed with the system losses. In future work, the active damping method in order to expand the stable operation area and the parameter design method will be provided.

## Appendix

Each element of the state equation (3) are expressed as follows.

$$A_{11}=\frac{-1}{1-\dfrac{L_{bus}{}^2}{(L_{bus}+L_{b1})(L_{bus}+L_{b2})}}\frac{R_{bus}+R_{b1}}{L_{bus}+L_{b1}}\left(1-\frac{L_{bus}R_{bus}}{(R_{bus}+R_{b1})(L_{bus}+L_{b1})}\right) \tag{15}$$

$$A_{12}=\frac{-1}{1-\dfrac{L_{bus}{}^2}{(L_{bus}+L_{b1})(L_{bus}+L_{b2})}}\frac{1}{L_{bus}+L_{b1}} \tag{16}$$

$$A_{15}=\frac{-1}{1-\dfrac{L_{bus}{}^2}{(L_{bus}+L_{b1})(L_{bus}+L_{b2})}}\frac{R_{bus}}{L_{bus}+L_{b1}}\left(1-\frac{L_{bus}(1+R_{b2}/R_{bus})}{(L_{bus}+L_{b2})}\right) \tag{17}$$

$$A_{16}=\frac{-1}{1-\dfrac{L_{bus}{}^2}{(L_{bus}+L_{b1})(L_{bus}+L_{b2})}}\frac{L_{bus}}{(L_{bus}+L_{b1})(L_{bus}+L_{b2})} \tag{18}$$

$$A_{21}=1/C_{b1} \tag{19}$$

$$A_{23}=-1/C_{b1} \tag{20}$$

$$A_{32}=\frac{1}{L_m}\left(\alpha_1{}^2-\frac{K_pI_{b1,0}}{V_{dc}}\right) \tag{21}$$

Table 2 Experimental condition.

| Circuit | | |
|---|---|---|
| $L_{bus}$ | Wiring indutance of DC Bus | 10 mH |
| $R_{bus}$ | Wiring resistance of DC Bus | 1.8 Ω |
| $C_{b1}$, $C_{b2}$ | Inverter input capasitance | 6.8 μF |
| $V_{dc}$ | DC bus voltage | 280 V |
| $f_{sw}$ | Switching frequency | 20 kHz |
| $T_d$ | Dead time | 2 μs |
| Drive Side Motor (Unit #1, #2) | | |
| R88M-1M40030T (Omron) | | |
| Load Side Motor (Unit #1, #2) | | |
| SGMJV-08ADA21 (YASKAWA Electric Corporation) | | |

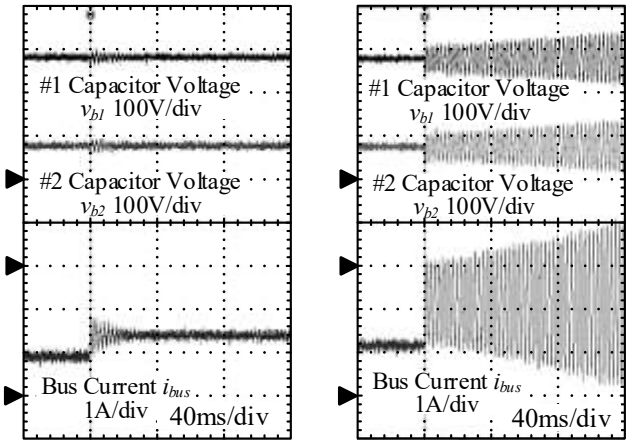


(a)Stable condition. (b)Unstable condition.

Fig. 11 The waveform of the bus current $i_{bus}$ and the input capacitor voltage on each unit $v_{b1}$, $v_{b2}$ in an unstable condition. The oscillation occurs when the system is unstable.

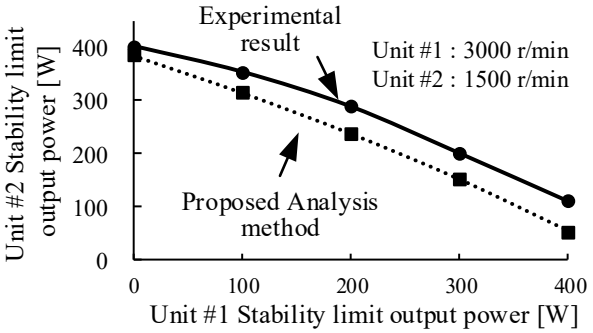


Fig. 12 The comparison of stability limit between the proposed analysis method and experiment when two servo drivers are driven.

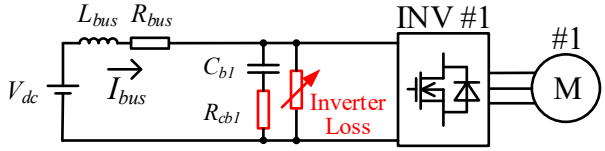


Fig. 13 The simulation circuit model. The model includes the ESR of the input capacitor and the variable resistance as the inverter loss.

$$A_{33}=-\frac{R_a+K_p}{L_m} \tag{22}$$

$$A_{34}=1/L_m \tag{23}$$

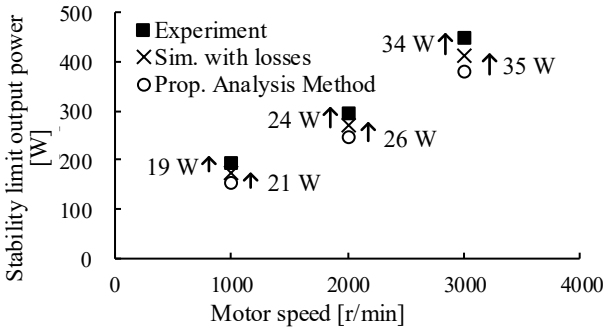


Fig. 14 The comparison of stability limit by the proposed method, the simulation with losses, and the experiment according to motor speeds. The error between the simulation result and the experimental result is reduced than the error between the analysis result and the experimental by approximately 50%.

$$A_{42} = -\frac{K_p I_{b1,0}}{T_i V_{dc}} \tag{24}$$

$$A_{43} = -\frac{K_p}{T_i} \tag{25}$$

$$A_{51} = \frac{-1}{1-\dfrac{L_{bus}{}^2}{(L_{bus}+L_{b1})(L_{bus}+L_{b2})}} \frac{R_{bus}}{L_{bus}+L_{b2}} \left(1-\frac{L_{bus}(1+R_{b1}/R_{bus})}{(L_{bus}+L_{b1})}\right) \tag{26}$$

$$A_{52} = \frac{-1}{1-\dfrac{L_{bus}{}^2}{(L_{bus}+L_{b1})(L_{bus}+L_{b2})}} \frac{L_{bus}}{(L_{bus}+L_{b1})(L_{bus}+L_{b2})} \tag{27}$$

$$A_{55} = \frac{-1}{1-\dfrac{L_{bus}{}^2}{(L_{bus}+L_{b1})(L_{bus}+L_{b2})}} \frac{R_{bus}+R_{b2}}{L_{bus}+L_{b2}} \left(1-\frac{L_{bus}R_{bus}}{(R_{bus}+R_{b2})(L_{bus}+L_{b2})}\right) \tag{28}$$

$$A_{56} = \frac{-1}{1-\dfrac{L_{bus}{}^2}{(L_{bus}+L_{b1})(L_{bus}+L_{b2})}} \frac{1}{L_{bus}+L_{b2}} \tag{29}$$

$$A_{65} = 1/C_{b2} \tag{30}$$

$$A_{67} = -1/C_{b2} \tag{31}$$

$$A_{76} = \frac{1}{L_m}\left(\alpha_2{}^2 - \frac{K_p I_{b2,0}}{V_{dc}}\right) \tag{32}$$

$$A_{77} = -\frac{R_a + K_p}{L_m} \tag{33}$$

$$A_{78} = 1/L_m \tag{34}$$

$$A_{86} = -\frac{K_p I_{b2,0}}{T_i V_{dc}} \tag{35}$$

$$A_{43} = -\frac{K_p}{T_i} \tag{36}$$

$$B_1 = \frac{1}{1-\dfrac{L_{bus}{}^2}{(L_{bus}+L_{b1})(L_{bus}+L_{b2})}} \frac{1}{L_{bus}+L_{b1}} \left(1-\frac{L_{bus}}{L_{bus}+L_{b2}}\right) \tag{37}$$

$$B_1 = \frac{1}{1-\dfrac{L_{bus}{}^2}{(L_{bus}+L_{b1})(L_{bus}+L_{b2})}} \frac{1}{L_{bus}+L_{b2}} \left(1-\frac{L_{bus}}{L_{bus}+L_{b1}}\right) \tag{38},$$

where $\alpha_1$ and $\alpha_2$ are the conversion ratio from the bus voltage to the output voltage of each unit, $I_{b1,0}$ and $I_{b2,0}$ are the steady-state value of each DC-link current.

## REFERENCES


[1] N. Nakao, K. Tobari, T. Sugino, Y. Ito, M. Mishima, and D. Maeda, “Torque Ripple Suppression for PMSMs using Feedforward Compensation and Online Parameter Estimation”, in *IEEJ Journal of Industry Applications*, Vol. 10, No. 4, pp. 497-505(2021).

[2] M. Kakihara, M. Takaki, M. Ohto, and S. Morimoto, "Investigation of Servomotor Structure for Sensorless Control Based on High-Frequency Injection Method", in *IEEJ Journal of Industry Applications*, Vol. 10, No. 6, pp. 718-725 (2021)

[3] N. Kawamura, T. Zanma, K. Koiwa, K. Liu, and M. Hasegawa, "Position Sensorless Adaptive Positioning Servo System with Simplified Differential Calculation and High-Frequency Voltage Injection Strategy Considering Acoustic Noise Suppression", in *IEEJ Journal of Industry Applications*, Vol. 10, No. 1, pp. 1-10 (2021)

[4] E. Totoki, S. Yamaguchi, T. Tanaka, K. Ito, A. Daikoku, and S. Morimoto, "Torque Ripple Reduction for Permanent Magnet Motor using New Configuration for Concentrated Windings", in *IEEJ Journal of Industry Applications*, Vol. 11, No. 3, pp. 531-537 (2022)

[5] T. Kai, H. Sekiguchi, and H. Ikeda, "Control Structure with Dual Acceleration Feedback for Positioning Machine with Semi-Closed Servo System", in *IEEJ Journal of Industry Applications*, Vol. 11, No. 2, pp. 351-358 (2022)

[6] T. Kiribuchi, T. Zaitsu, M. Doi, K. Kusaka, and J. Itoh, “DC-bus System for Servo Drives and its Stability Analysis,” in *IEEE International Conference on DC Microgrids 2019*, No. 7-A-3 (2019)

[7] Y. Gu, W. Li, and X. He: "Passivity-Based Control of DC Microgrid for Self-Disciplined Stabilization", in *IEEE Transaction on Power Systems*, Vol. 30, No. 5, pp. 2623-2632 (2015)

[8] N. Zhao, G. Wang, R. Zhang, B. Li, Y. Bai, and D. Xu, "Inductor Current Feedback Active Damping Method for Reduced DC-Link Capacitance IPMSM Drives", in *IEEE Transaction on Power Electronics*, Vol. 34, No. 5, pp. 4558-4568 (2019)

[9] X. Wang, R. Yao, and F. Rao, "Three-Step Impedance Criterion for Small-Signal Stability Analysis in Two-Stage DC Distributed Power Systems", in *IEEE Power Electronics Letters*, Vol. 1, No. 3, pp. 83-87(2003)

[10] J. Lee, G. Lee, S. Park, and R. Kim: "Impedance-Based Modeling and Common Bus Stability Enhancement Control Algorithm in DC Microgrid", in *IEEE Access*, Vol. 8, pp. 211224-211234 (2020)

[11] X. Feng, J. Liu, and F. C. Lee, "Impedance Specifications for Stable DC Distribution Power Systems", in *IEEE Transaction on Power Electronics*, Vol. 17, No. 2, pp. 157-162 (2002)

[12] Y. Jeung, D. Lee, T. Dragicevic, and F. Blaabjerg, "Design of Passivity-Based Damping Controller for Suppressing Power Oscillations in DC Microgrids", in *IEEE Transaction on Power Electronics*, Vol. 36, No. 4, pp. 4016-4028 (2021)

[13] A. Riccobono and E. Santi, "Comprehensive Review of Stability Criteria for DC Power Distribution Systems", in *IEEE Transaction on Industry Applications*, Vol. 50, No. 5, pp. 3525-3535 (2014)

[14] K. Kusaka, N. Takaoka, T. Sakuraba, H. Watanabe, and J. Itoh, "Single-Phase AC Grid-Tied Inverter with Buck-Type Active Power Decoupling Circuit Operated in Discontinuous Current Mode", in *IEEJ Journal of Industry Applications*, Vol. 10, No. 3, pp. 292-302(2021)

[15] W. Lee, and S. Sul, "DC-Link Voltage Stabilization for Reduced DC-Link Capasitor Inverter", in *IEEE Transaction on Industry Applications*, Vol. 50, No. 1, pp. 404-414 (2014)

[16] N. Zhao, G. Wang, D. Xu, and D. Xiao, "An Active Damping Control Method for Reduced DC-Link Capacitance IPMSM Drives", in *IEEE Transaction on Industrial Electronics*, Vol. 65, No. 3, pp. 2057-2068 (2018)

[17] R.D. Middlebrook: “Input Filter Considerations in Design and Application of Switching Regulators”, in *Proc. of IEEE Industrial Application Society Annual Meeting*, pp. 366-382(1976)